crystals

MDPI

Article

The Structure and Optical Properties of Luminescent Terbium Terephthalate Metal–Organic Frameworks Doped with Yttrium, Gadolinium, and Lanthanum Ions

Anna S. Petrova [1], Oleg S. Butorlin [1], Yulia N. Toikka [1], Ilya E. Kolesnikov [1], Sergey N. Orlov [1,2], Mikhail N. Ryazantsev [1,3], Nikita A. Bogachev [1], Mikhail Yu. Skripkin [1] and Andrey S. Mereshchenko [1,*]

[1] Saint Petersburg State University, 7/9 Universitetskaya emb., Saint Petersburg 199034, Russia; an.petra04.floreo@gmail.com (A.S.P.); olbuse@mail.ru (O.S.B.); helmi24@mail.ru (Y.N.T.); ilya.kolesnikov@spbu.ru (I.E.K.); orlov.s.n.1989@yandex.ru (S.N.O.); mikhail.n.ryazantsev@gmail.com (M.N.R.); n.bogachev@spbu.ru (N.A.B.); skripkin1965@yandex.ru (M.Y.S.)
[2] Institute of Nuclear Industry, Peter the Great St. Petersburg Polytechnic University (SPbSU), 29, Polytechnicheskaya Street, Saint Petersburg 195251, Russia
[3] Nanotechnology Research and Education Centre RAS, Saint Petersburg Academic University, ul. Khlopina 8/3, Saint Petersburg 194021, Russia
* Correspondence: a.mereshchenko@spbu.ru; Tel.: +7-951-677-5465

Abstract: The structural features and luminescent properties of heterometallic Tb–Gd, Tb–La, and Tb–Y terephthalate metal–organic frameworks, namely $(Tb_xM_{1-x})_2(1,4\text{-bdc})_3 \cdot 4H_2O$ (M = Gd, La, Y), were studied in detail in a wide concentration range (x = 0.001–1). The crystalline phase of synthesized compounds corresponds to $Ln_2(1,4\text{-bdc})_3 \cdot 4H_2O$. The lifetime of $^5D_4$ decreased with increased Tb^{3+} concentration, but PLQY depends non-linearly on the Tb^{3+} concentration. The 50% substitution of Tb^{3+} for Y^{3+}, Gd^{3+}, or La^{3+} ions result in the significant enhancement of photoluminescence quantum yield, up to 1.6 times. The morphology, thermal stability, and vibrational structure of the selected homo- and bi-metallic materials is reported as well.

Keywords: metal–organic framework; luminescence; rare earth; terbium; gadolinium; lanthanum; yttrium; antenna effect

Citation: Petrova, A.S.; Butorlin, O.S.; Toikka, Y.N.; Kolesnikov, I.E.; Orlov, S.N.; Ryazantsev, M.N.; Bogachev, N.A.; Skripkin, M.Y.; Mereshchenko, A.S. The Structure and Optical Properties of Luminescent Terbium Terephthalate Metal–Organic Frameworks Doped with Yttrium, Gadolinium, and Lanthanum Ions. *Crystals* **2024**, *14*, 966. https://doi.org/10.3390/cryst14110966

Academic Editor: Thomas Schleid

Received: 16 October 2024
Revised: 29 October 2024
Accepted: 5 November 2024
Published: 8 November 2024

1. Introduction

Metal–organic frameworks (MOFs) are porous materials consisting of networks of metal ions or clusters connected to each other with organic ligands with several donor atoms. These materials have received much attention in the last two decades due to their pronounced crystallinity, porosity, high stability, and diversity in structures and topologies. Rare earth element (REE)-based MOFs are of particular relevance, since their luminescent properties strongly depend on the type of lanthanide ion. The development of REE-based MOFs that exhibit strong luminescent properties is a relevant and promising area of research. These REE-MOFs can be used in LEDs, luminescent sensors, contrast agents for imaging, catalysts, and analytical tools to detect harmful substances in food, drinking water, and the environment [1–9]. Compounds based on europium and terbium are particularly popular due to their bright red and green light emission, respectively. Thus, OLEDs based on metal–organic terbium compounds were recently reported in numerous works [10–13]. In addition, heavy metal ions efficiently quench the photoluminescence of Tb^{3+} compounds, such as mercury, bismuth, and chromium, as well by organic substances such as gossypol, acetone, sulfamerazine, and other molecules [14–18], which indicates Tb^{3+} compounds as promising materials for the development of luminescent turn-off sensors for the abovementioned compounds.

The direct photoexcitation of lanthanide ions is inefficient because 4f–4f transitions are not allowed according to Laporte's rule. This challenge can be overcome by employing

energy transfer from an electronically excited ligand to one of the atomic level of the lanthanide ion ("antenna effect") [19–21]. The "antenna" organic ligands usually possess high UV extinction coefficients, strongly coordinate with REE ions, and efficiently transfer energy to REE ions. Accordingly, aromatic carboxylates, such as 1,4-benzenedicarboxylate (terephthalate, 1,4-bdc) and their various derivatives, have become the most frequently used ligands [22–25].

The presence of both luminescent and non-luminescent ions of rare earth elements in REE-MOFs can have a substantial impact on the structural and optical properties of these compounds. The doping effect on the structure of heterometallic REE–metal–organic frameworks (MOFs) has been explored in multiple studies. Usually, the crystalline structure is not alternated when a small fraction of one lanthanide is substituted for another one in the same oxidation state. The significant doping amount by another lanthanide ion, however, can result in crystalline phase change. Thus, Jarley Nascimento et al. demonstrated [26] that the compounds $Gd_{1-x}Eu_x(1,4\text{-bdc})_3(dmf)_2(H_2O)_n$ (dmf—dimethylformamide; x = 0.01, 0.03, 0.05, 0.07, 0.09) are isostructural, with $[Eu_2(1,4\text{-bdc})_3(dmf)_2(H_2O)]$ at the Eu^{3+} content between 1 and 7 at.%. Meanwhile, at the Eu^{3+} concentration of 9 at.%, the obtained material possessed a structure of $[Eu_2(1,4\text{-bdc})_3(dmf)_2(H_2O)_2]$. In our previous works, we observed the crystalline phase alternation in $(Eu_xLu_{1-x})_2(1,4\text{-bdc})_3{\cdot}nH_2O$ and $(Tb_xLu_{1-x})_2(1,4\text{-bdc})_3{\cdot}nH_2O$ MOFs [27–30]. Substitution of up to 90% of Eu^{3+} or Tb^{3+} by Lu^{3+} ions does not affect the crystalline phase of the resulting compounds, $Ln_2(1,4\text{-bdc})_3{\cdot}4H_2O$, which is isostructural to europium and terbium terephthalates, namely $Eu_2bdc_3{\cdot}4H_2O$ and $Tb_2bdc_3{\cdot}4H_2O$, correspondingly. At a lutetium content of more than 98%, the synthesized compounds possessed a $Ln_2(1,4\text{-bdc})_3$, $Ln_2(1,4\text{-bdc})_3{\cdot}10H_2O$, or $Ln_2(1,4\text{-bdc})_3{\cdot}2.5H_2O$ crystalline phase depending on the concentration of the initial reagents. We observed that the particle morphology and optical properties, such as fine structure of emission spectra, photoluminescence quantum yields (PLQY), and lifetime values, are more significantly affected by the crystalline phase than by the concentration of the luminescent lanthanide ion (Eu^{3+} or Tb^{3+}). In spite of the fact that the alternation of the crystalline phase significantly affects the photoluminescence of REE-MOFs, the optical properties of heterometallic MOFs also depend on the concentration of the luminescent ion within one crystalline phase in cases of isomorphic substitution of the luminescent REE ion to the optically inactive one. However, only a few studies have studied such concentration dependences. In our previous work, for $(Eu_xM_{1-x})_2(1,4\text{-bdc})_3{\cdot}4H_2O$ (M = Gd, La, Y) MOFs, we demonstrated that, at larger Eu^{3+} concentrations, for the Eu–Y and Eu–La series, PLQY remains the same (about 9–11%), whereas in the Eu–Gd series, it reaches a maximum of 15% at the Eu^{3+} content of 10 at.% and then slightly decreases, reaching 10% in homometallic europium(III) terephthalate [31]. Utochnikova et al. previously reported the Gd^{3+} and Y^{3+} doping effect on the optical properties of heterometallic solid solutions of $(Tb_xY_{1-x})_2(1,4\text{-bdc})_3(H_2O)_4$ and $Eu_xGd_{1-x}(dbm)_3(phen)$ (dbm—dibenzoylmethanate, phen—o-phenantroline) MOFs [24]. A steep increase in quantum yield was observed at the low concentration regions of Eu^{3+} or Tb^{3+} ions. For the abovementioned heterometallic coordination polymers, when the concentration of luminescent ions (Tb^{3+} or Eu^{3+}) exceeded 20%, the quantum yield remains the same; meanwhile, the excited state lifetime decreases with increasing concentrations of the luminescent ion [32]. However, the structural features were not studied in detail in the mentioned study [32], and the authors studied the doping effect only by one REE, namely Y^{3+} in cases of Tb^{3+}-based terephthalates. Bimetallic terephthalates of equimolar compositions are reported by Tarek Alammar et al. [33]. The authors studied the several heterometallic terephthalates, namely $(Ln_{0.5}Gd_{0.5})_2(1,4\text{-bdc})_3{\cdot}4H_2O$ (M = Eu, Tb, Sm). Despite their detailed analysis of the optical properties of these compounds, this work considered the dilution of only one non-luminescent ion (gadolinium) and only in one concentration. In the article by Victor Haquin et al. [34], the researchers investigated the systems $(Tb_xM_{1-x})_2(1,4\text{-bdc})_3{\cdot}4H_2O$ (M = Y, La, Gd) for their fluorescent and structural properties. However, in their work, more attention was paid to tri-metallic systems and systems containing Eu^{3+} and Tb^{3+},

and bimetallic systems with luminescent and non-luminescent ions were viewed fluently. The authors give a large series of synthesized compounds of the series $(Tb_xGd_{1-x})_2$(1,4-bdc)$_3 \cdot 4H_2O$ (x = 0.05–100), the details of their optical properties on selected samples, and luminescence spectra for all. At the same time, the series containing Y and La has received much less attention; for lanthanum (III)'s intensity of luminescence, there is no information for yttrium (III). In our work, we not only expanded the range of concentrations towards their reduction (x = 0.001–0.04), but also studied in detail the structural features, morphology, vibration structure, thermal stability, fine structure of the emission bands, excited state kinetics, and photoluminescence quantum yields. It is worth noting that our measurement results differ from those presented in the previous work, and the goal of our work is to carefully demonstrate the dependence of the above properties of the terephthalate of the terbium (III) on the degree and nature of substitution by ions of optically inactive rare earth elements.

Thus, in the current work, we studied in detail the doping effect of the various non-luminescent ions (Y^{3+}, Gd^{3+}, and La^{3+}) both on the structure and on the luminescent properties of Tb^{3+}-based heterometallic terephthalates $(Tb_xM_{1-x})_2$(1,4-bdc)$_3 \cdot 4H_2O$ (M = Gd, La, Y; x = 0.001–1) in a wide concentration range, and, contrary to previous work [32], demonstrated that 50% substitution of Tb^{3+} for Y^{3+}, Gd^{3+}, or La^{3+} ions results in the significant enhancement of photoluminescence quantum yields, up to 1.6 times. Also, morphology, thermal stability, and vibrational structure of the selected homo- and bi-metallic materials is reported.

2. Materials and Methods

Terbium (III) chloride hexahydrate, yttrium (III) chloride hexahydrate, gadolinium (III) chloride hexahydrate, and lanthanum (III) chloride hexahydrate were purchased from Chemcraft (Kaliningrad, Russia). 1,4-benzenedicarboxylic (terephtalic, H_2(1,4-bdc)) acid (>98%), sodium hydroxide (>99%), nickel (II) chloride hexahydrate (>99%), and EDTA disodium salt (0.1 M aqueous solution), and murexide were purchased from Sigma-Aldrich Chemie GmbH (Taufkirchen, Germany) and used without additional purification.

The heterometallic terephthalate compounds with a general formula of $(Tb_xM_{1-x})_2$(1,4-bdc)$_3 \cdot 4H_2O$ (M = Y, Gd, La) were prepared by mixing 0.2 M $TbCl_3$ and 0.2 M MCl_3 (M = Y, La, or Gd) with 2 mL of 0.3 M Na_2(1,4-bdc) aqueous solution. The $TbCl_3$ and MCl_3 solutions were mixed in stoichiometric amounts, and the total volume of the solutions was 1 mL. The resulting white precipitates were separated from the mixture using centrifugation at 4000× *g* and washed three times with deionized water. The samples were then dried at 60 °C. The Tb^{3+}/M^{3+} (M = Y, Gd, La) ratios in the heterometallic terephthalates were confirmed using energy-dispersive X-ray spectroscopy (EDX) (EDX spectrometer EDX-800P, Shimadzu, Japan). The Tb/M (M = Y, Gd, La) ratios obtained from EDX were consistent with the expected ratios of Tb^{3+}/M^{3+} (M = Y, Gd, La) taken for the synthesis for Tb^{3+} content within 1 at.% accuracy. X-ray powder diffraction (XRD) measurements were performed with a D2 Phaser (Bruker, Billerica, MA, USA) X-ray diffractometer using Cu Kα radiation (λ = 1.54056 Å). SEM images were obtained using a scanning electron microscope Zeiss Merlin. Thermogravimetry curves were obtained using a TG 209 F1 Libra thermo-microbalance (Netzsch, Hanau, Germany). The measurement of FTIR spectra was carried out using the IRAffinity-1 spectrometer (Shimadzu, Kyoto, Japan). To carry out photoluminescence studies, the synthesized samples (20 mg) and potassium bromide (300 mg) were pressed into pellets (diameter 13 mm). The photoluminescence data were obtained with a Fluoromax-4 fluorescence spectrometer (Horiba Jobin Yvon, Kyoto, Japan) in perpendicular geometry. Lifetime measurements were performed with the same spectrometer using a pulsed Xe lamp (pulse duration: 3 μs) in a timescale of 50 μs–10 ms. The absolute values of the photoluminescence quantum yields were recorded using a Fluorolog-3 Quantaphi-2 (Horiba Scientific, Kyoto, Japan) device using an integration sphere. All measurements were performed at 25 °C.

3. Results

3.1. Structure and Morphology

The powder X-ray diffraction (PXRD) patterns of the synthesized compounds $(Tb_xM_{1-x})_2$(1,4-bdc)$_3\cdot nH_2O$ (M = Y, La, Gd) are shown in Figure 1a (main text) and Figure S1 (Supplementary Materials). The analysis of XRD patterns demonstrates that all synthesized compounds possess the Ln_2(1,4-bdc)$_3\cdot 4H_2O$ crystalline phase (Ln = Ce–Yb) [35]. In this structure, the lanthanide ions have coordination number six and are connected to oxygen atoms of two water molecules and six different terephthalate ions. The polyhedron of these oxygen atoms forms a distorted square antiprism around a metal ion.

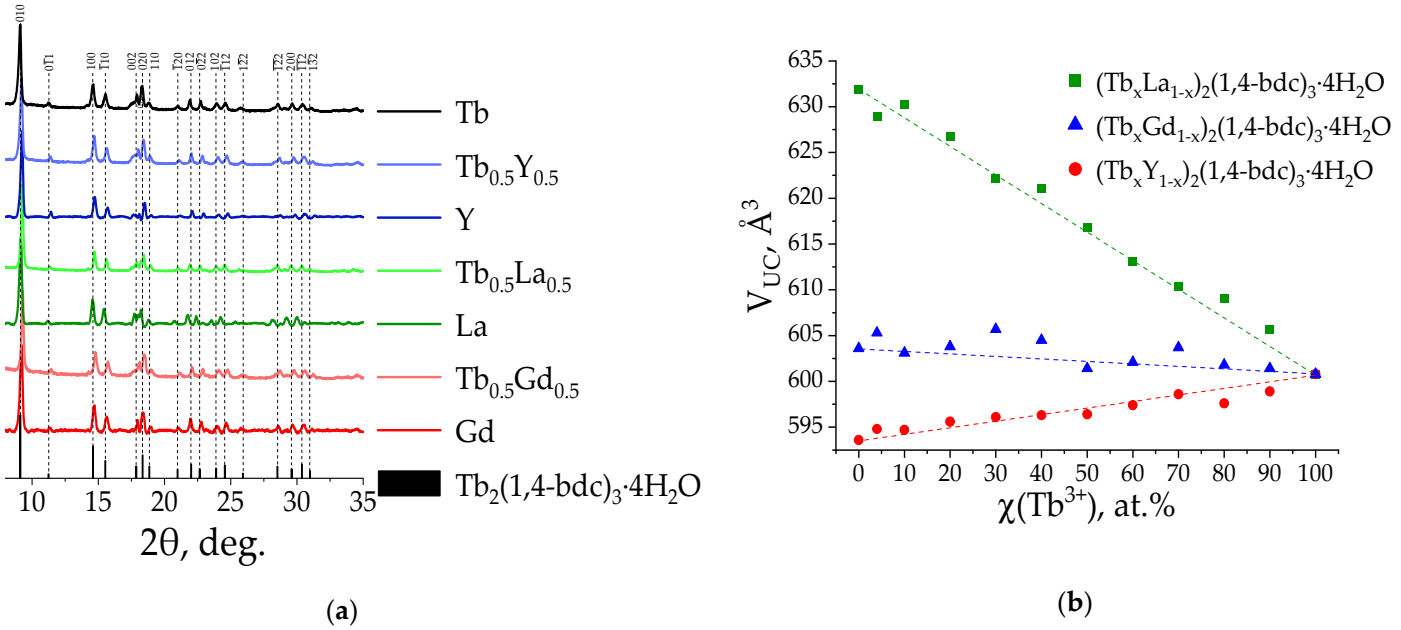

Figure 1. The PXRD patterns of selected $(Tb_xM_{1-x})_2$(1,4-bdc)$_3\cdot 4H_2O$ (M = Y, La, Gd; x = 0, 0.01, 0.1, 1) and the simulated XRD pattern of Tb_2(1,4-bdc)$_3\cdot 4H_2O$ single-crystal structure were taken from ref. [35] (**a**) and unit cell volume ($V_{u.c.}$) concentration dependence refined for $(Tb_xM_{1-x})_2$(1,4-bdc)$_3\cdot 4H_2O$ (M = Gd, La, Y) (**b**).

The unit cell parameters of synthesized compounds were refined, and the unit cell volumes were calculated at different Tb^{3+} concentrations from 0 to 100 at.%. Unit cell parameters of the samples were refined using the Pawley method from the PXRD data (Table S1, Supplementary Materials) [36]. The unit cell volumes were calculated from unit cell parameters. We have found that Vegard's law is obeyed in the studied systems because unit cell volumes linearly depend on the Tb^{3+} content (Figure 1b) [37]. Therefore, the $(Tb_xM_{1-x})_2$(1,4-bdc)$_3\cdot 4H_2O$ (M = Y, La, Gd) terephthalates can be considered as solid solutions in a whole concentration range. For the $(Tb_xLa_{1-x})_2$(1,4-bdc)$_3\cdot 4H_2O$, the increase in La^{3+} content results in the unit cell volume elevation due to a larger ionic radius of La^{3+} ions (1.160 Å, the coordination number is eight) than the ionic radius of Tb^{3+} ions (1.040 Å) [38]. The ionic radius of the Gd^{3+} (1.053 Å) and Tb^{3+} ions are close to each other, which leads to close values of unit cell parameters among $(Tb_xGd_{1-x})_2$(1,4-bdc)$_3\cdot 4H_2O$ series. In the $(Tb_xM_{1-x})_2$(1,4-bdc)$_3\cdot 4H_2O$ series, the substitution of larger Tb^{3+} by smaller Y^{3+} (0.977 Å) ions results in a decrease in unit cell volume.

The particle morphology and the porosity of the selected synthesized materials such as $(Tb_{0.5}M_{0.5})_2$(1,4-bdc)$_3\cdot 4H_2O$ (M = Gd, La, Y) were revealed using scanning electron microscopy (SEM). The pore and nanoparticle sizes were estimated from the SEM images. SmartTiffV2 software (V02.00) allows for distance estimations on .tif images obtained as scanning electron microscopy output files on the instrument. The SEM images (Figure 2) clearly demonstrate that the resulting compounds consist of large particles sized between 5 and 20 μm. The obtained material has a porous structure with pore size of

10–200 nm. One can observe that large particles consist of aggregated spindle-shaped or filiform nanoparticles.

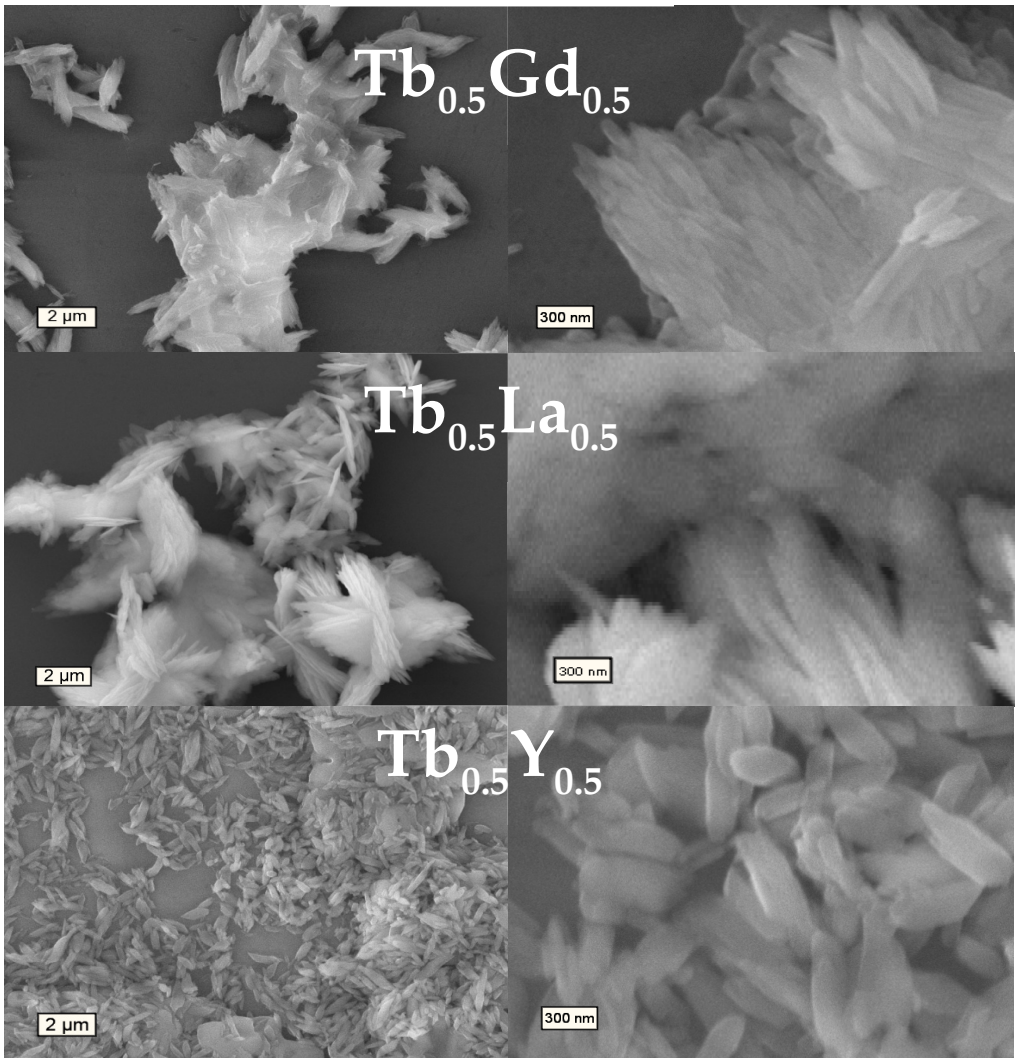

Figure 2. SEM images of $(Tb_{0.5}M_{0.5})_2(1,4\text{-bdc})_3 \cdot 4H_2O$ (M = Gd, La, Y).

3.2. Vibrational Spectroscopy

The IR spectra of the selected homometallic $M_2(1,4\text{-bdc})_3 \cdot 4H_2O$ (M = Y, Gd, La, Tb) and heterometallic $(Tb_{0.5}M_{0.5})_2(1,4\text{-bdc})_3 \cdot 4H_2O$ (M = Y, Gd, La) terephthalates (Figure 3) were measured in order to follow the doping effect on the vibrational structure of the ligand. The broad band peaking at about 3500 cm^{-1} corresponds to the O–H stretching vibrations of lanthanide-coordinated water molecules. The 1270–1470 and 1470–1800 cm^{-1} narrow bands correspond to the C–O symmetric and asymmetric stretching vibrations of the carboxyl group in the terephthalate ion, respectively. The results obtained are consistent with the literature data on rare earth terephthalates [39,40]. All of the studied compounds have almost identical IR spectra that agree with PXRD data, which demonstrates that all of the synthesized compounds have the same crystalline phase, namely $Ln_2(1,4\text{-bdc})_3 \cdot 4H_2O$.

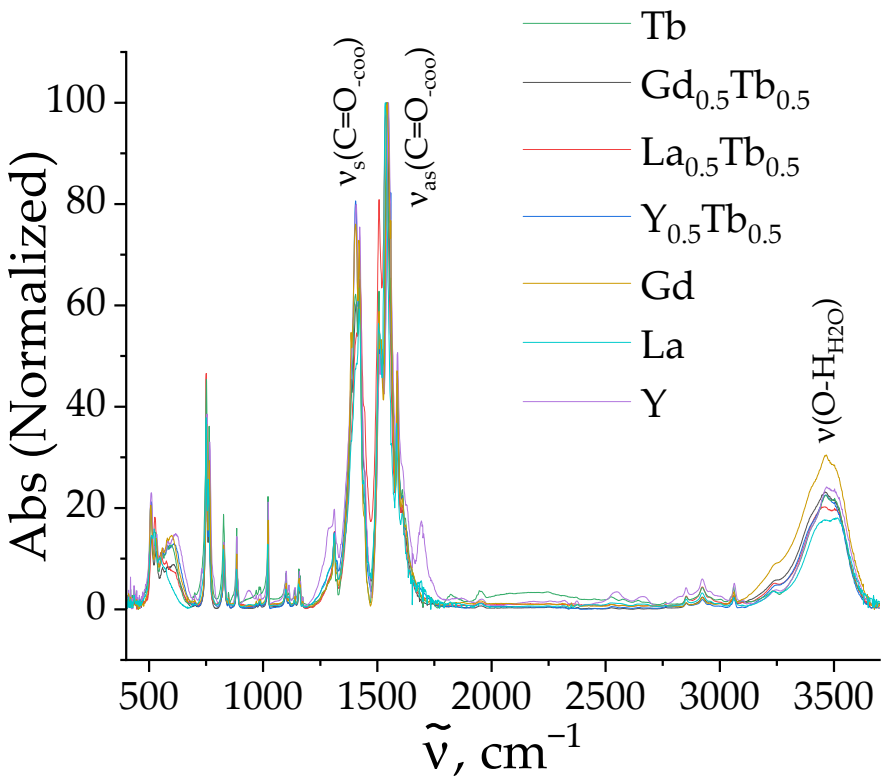

Figure 3. IR spectra of $(Tb_{0.5}M_{0.5})_2(1,4\text{-bdc})_3 \cdot 4H_2O$ and $M_2(1,4\text{-bdc})_3 \cdot 4H_2O$ (M = Y, Gd, La, Tb).

3.3. Thermogravimetric Analysis

Thermogravimetric analysis (TGA) curves measured in the temperature range of 35–200 °C the selected homometallic $M_2(1,4\text{-bdc})_3 \cdot 4H_2O$ (M = Y, Gd, La, Tb) and heterometallic $(Tb_{0.5}M_{0.5})_2(1,4\text{-bdc})_3 \cdot 4H_2O$ (M = Y, Gd, La) terephthalates are shown in Figure 4. For all of the studied samples, a weight loss of 8.0–9.3% was recorded ranging between 100 °C and 160 °C. As indicated earlier [41], the weight loss at such temperatures corresponds to the dehydration process of the compounds according to the following equation:

$$M_2(1,4\text{-bdc})_3 \cdot 4H_2O = M_2(1,4\text{-bdc})_3 + 4H_2O \text{ or}$$

$$(Tb_{0.5}M_{0.5})_2(1,4\text{-bdc})_3 \cdot 4H_2O = (Tb_{0.5}M_{0.5})_2(1,4\text{-bdc})_3 + 4H_2O$$

The mass loss of 8.0–9.3% corresponds to the elimination of 3.8–4.2 water molecules from the initial terephthalates. These data are consistent with the results of the PXRD, which showed that all of the studied materials crystallize in the $Ln_2(1,4\text{-bdc})_3$ $4H_2O$ phase. The temperature of the dehydration ($T_{deh.}$) of $M_2(1,4\text{-bdc})_3 \cdot 4H_2O$ (M = Y, Gd, La, Tb) and $(Tb_{0.5}M_{0.5})_2(1,4\text{-bdc})_3 \cdot 4H_2O$ (M = Y, Gd, La) is presented in Table 1. As we can see, $T_{deh.}$ increases with increases in the ionic radius and, respectively, the unit cell of the compounds. We also observe that the dehydration temperatures of heterometallic terephthalates are in the range between the temperatures of monometallic terephthalates. A correlation exists between the dehydration temperatures and the unit cell volume of the samples. As the unit cell volume decreases, the free volume available for the four water molecules also decreases or disappears. Considering the volume of a single water molecule to be approximately 6 $Å^3$ (24 $Å^3$ for four molecules), we observe a volume change of about 39 $Å^3$ when moving from lanthanum to yttrium, exceeding the volume required by the water molecules. This suggests that the surrounding molecules exert additional pressure on the water molecules. Under this pressure, water molecules are more likely to leave the system, resulting in a lower dehydration temperature for materials with smaller unit cell volumes compared to those with larger unit cell volumes.

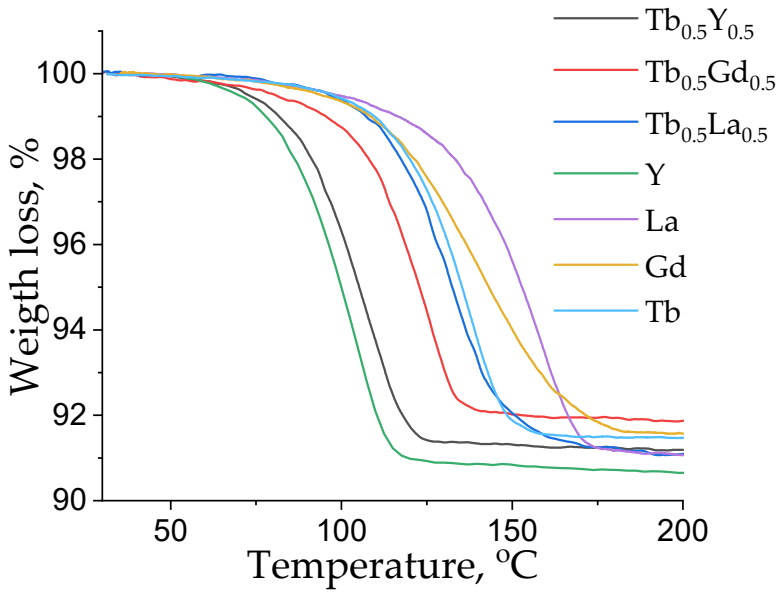

Figure 4. TGA curves of selected heterometallic $(Tb_{0.5}M_{0.5})_2(1,4\text{-bdc})_3 \cdot 4H_2O$ (M = Gd, La, Y) and homometallic $M_2(1,4\text{-bdc})_3 \cdot 4H_2O$ (M = Tb, Gd, La, Y) terephthalates measured in the temperature range of 35–200 °C.

Table 1. Temperatures of the dehydration for selected heterometallic $(Tb_{0.5}M_{0.5})_2(1,4\text{-bdc})_3 \cdot 4H_2O$ (M = Gd, La, Y) and homometallic $M_2(1,4\text{-bdc})_3 \cdot 4H_2O$ (M = Tb, Gd, La, Y) terephthalates.

Compound	$T_{deh.}$, °C
$Y_2(1,4\text{-bdc})_3 \cdot 4H_2O$	104.8
$Tb_2(1,4\text{-bdc})_3 \cdot 4H_2O$	120.1
$Gd_2(1,4\text{-bdc})_3 \cdot 4H_2O$	142.5
$La_2(1,4\text{-bdc})_3 \cdot 4H_2O$	158.9
$TbY(1,4\text{-bdc})_3 \cdot 4H_2O$	108.3
$TbGd(1,4\text{-bdc})_3 \cdot 4H_2O$	126.3
$TbLa(1,4\text{-bdc})_3 \cdot 4H_2O$	132.6

3.4. Luminescent Properties

The emission spectra of the synthesized compounds are shown in Figure 5 (main text) and Figure S2 (Supplementary Materials). All emission spectra exhibit similar bands corresponding to the $^5D_4$–^7F_J (J = 3–6) f-f transitions of the Tb^{3+} ion: $^5D_4$–$^7F_3$ (623 nm), $^5D_4$–$^7F_4$ (584 nm), $^5D_4$–$^7F_5$ (546 nm), and $^5D_4$–$^7F_6$ (487 nm). The presence of characteristic Tb^{3+} bands in the emission spectra upon 320 nm excitation into the absorption band of terephthalate ion indicates the presence of an antenna effect. The initially populated singlet S_n state of the terephthalate ion undergoes a rapid internal conversion to the lowest-energy singlet S_1 state. The S_1 state effectively relaxes into the triplet T_1 state by intersystem crossing due to the presence of heavy lanthanide ion (heavy atom effect). The T_1 state of the terephthalate ion the $^5D_4$ energy level of the Tb^{3+} ion have close energies, resulting in an efficient energy transfer from the electronically excited terephthalate ion to the $^5D_4$ level of the Tb^{3+} ion [32,42]. The $^5D_4$ level Tb^{3+} ion then undergoes radiative transition to the underlying ^7F_J energy levels (J = 6, 5, 4, 3), which correspond to the narrow bands in the emission spectra of the studied compounds.

It is well known that the fine structure of the band splitting in the luminescence spectrum depends strongly on the local symmetry group of the luminescent lanthanide (III) ion. Thus, for europium ions, Binnemans reviews in detail the effect of local symmetry on the fine structure of the spectra [43]. The study of the symmetry of Tb^{3+} ions is conveniently interpreted through the study of the local symmetry of Eu^{3+} ions, the spectra of which contain convenient markers of the band structure [43], allowing us to draw a conclusion

about the symmetry group. Due to the close ionic radii, equality of charges, and close electron shells in the structure, we can say that when europium (III) ions are replaced by terbium (III) ions, there is no change in the local symmetry. As we have already shown, terephthalates are solid solutions where Vegard's law is fulfilled, and the isostructural substitution of some lanthanide ions for others leads only to a monotonic change in the unit cell parameters. Our previous studies have shown that $Eu_2(1,4\text{-bdc})_3{\cdot}4H_2O$ exhibits a $^5D_0$-$^7F_0$ transition [31], which, according to the Judd–Ofelt theory, is hidden and occurs only for coordination sites with C_n, C_{nv}, and C_s symmetry [41,43]. In the work by Daiguebonne et al., the authors report that lanthanide (III) ions had pseudo-C_4 symmetry in $Ln_2(1,4\text{-bdc}_3{\cdot}4H_2O$ (Ln = Tb, Eu) [41]. Therefore, we propose that a similar fine structure of emission bands indicates the identical pseudo-C_4 symmetry of metal ions in all of the studied materials, namely $(Tb_xM_{1-x})_2(1,4\text{-bdc})_3{\cdot}4H_2O$ (M = Y, La, Gd).

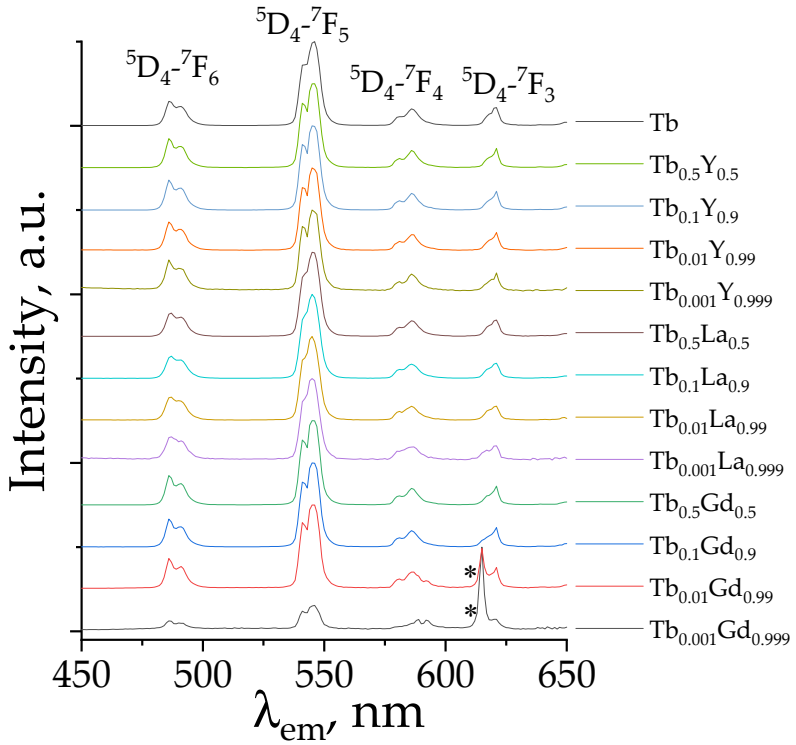

Figure 5. The normalized emission spectra of $(Tb_xM_{1-x})_2(1,4\text{-bdc})_3{\cdot}4H_2O$ (M = Y, La, Gd) at the selected Tb^{3+} concentrations (given in legend) upon 320 nm excitation. The artefact maxima peaking at 615 nm (marked as *) correspond to the Eu^{3+} present as impurities in the gadolinium nitrate used for the synthesis.

The fine structure of the emission spectra for the Y-, Gd-, and La-doped terephthalates is identical to that of the emission spectrum of unsubstituted terbium terephthalate, implying the same coordination environment of Tb^{3+} in the studied heterometallic compounds. This conclusion is in agreement with the PXRD data, which demonstrate isomorphic substitution of terbium by yttrium, gadolinium, and lanthanum ions among the studied series, $(Tb_xM_{1-x})_2(1,4\text{-bdc})_3{\cdot}4H_2O$ (M = Y, La, Gd). However, the concentration dependence of the integrated intensity of emission spectra (Table 2, main text, and Figure S3, Supplementary Materials) is non-monotonous as a result of non-monotonous photoluminescence quantum yield (PLQY) concentration dependence (Table 3). The photoluminescence decay curves of the $(Tb_xM_{1-x})_2(1,4\text{-bdc})_3{\cdot}4H_2O$ phosphors monitored at 546 nm ($^5D_4$–$^7F_5$ transition) are presented in Figure 6 ($\lambda_{ex.}$ = 320 nm). The photoluminescence decay curves were fitted by single exponential functions:

$$I(t) = I_0{\cdot}e^{-\frac{t}{\tau}},$$

where τ is the observed $^5D_4$ lifetime. We have found that the lifetime of the $^5D_4$ excited state decreases from 1.1 to 0.7 ms as the Tb^{3+} concentration increases (Table 3), which is consistent with our previous studies of Tb–Lu [28]. Lifetime depression is associated with the higher probability of energy transfer between close-located Tb^{3+} ions, as well as with the quenching of impurities at higher terbium content. The PLQYs of these compounds had maxima at about 50 at.% of Tb^{3+}, where the average PLQY is 63% (Table 2). The emission intensity and PLQY of REE-containing phosphors non-monotonously depend on the Tb^{3+} content, which is caused by the two competitive effects [44–47]. The number of luminescent sites increases as the Tb^{3+} content rises, which results in radiative emission probability elevation and, as a result, rises in emission intensity and PLQY. At the same time, the growth in Tb^{3+} concentration results in the distance shortage between the Tb^{3+} ions, leading to emission quenching [28]. As a result of this effect, the PLQY values of pure terbium terephthalate (100 at.% of Tb^{3+}) are lower than that of the MOFs, containing 50 at.% of Tb^{3+}.

Table 2. The value of the integrated intensity (*S*) of the luminescence spectra of $(Tb_xM_{1-x})_2(1,4\text{-bdc})_3{\cdot}4H_2O$ (M = Y, La, Gd).

χ(Tb^{3+}), at.%	***S* × 10^7, a.u.**		
	M = Gd	**M = La**	**M = Y**
0.1	3.99	4.01	2.50
0.2	4.69	3.32	4.16
0.4	9.16	6.17	6.84
0.6	10.02	9.46	8.51
0.8	9.87	10.92	1.01
1	15.26	10.06	7.96
2	13.26	15.97	15.56
4	10.40	22.58	35.00
6	42.02	24.21	43.95
8	58.79	30.00	44.57
10	36.87	31.40	64.56
20	56.62	33.10	46.84
30	32.05	22.64	52.51
40	50.33	20.87	43.18
50	69.91	31.31	47.53
60	50.38	38.78	42.33
70	57.49	38.96	42.80
80	60.45	38.29	48.83
90	35.23	27.22	34.12
100	38.18	23.52	36.10

Table 3. The observed $^5D_4$ lifetime and PLQYs of $(Tb_xM_{1-x})_2(1,4\text{-bdc})_3{\cdot}4H_2O$ (M = Y, La, Gd).

Compound	**χ(Tb^{3+}), at.%**	**τ, ms**	**PLQY, %**
$Tb_2(1,4\text{-bdc})_3{\cdot}4H_2O$	100	0.68 ± 0.01	46 ± 1
$(Tb_xY_{1-x})_2(1,4\text{-bdc})_3{\cdot}4H_2O$	1	1.10 ± 0.01	27 ± 1
	10	1.01 ± 0.01	57 ± 1
	50	0.93 ± 0.01	60 ± 1
	90	0.74 ± 0.01	48 ± 1
$(Tb_xLa_{1-x})_2(1,4\text{-bdc})_3{\cdot}4H_2O$	1	1.02 ± 0.01	24 ± 1
	10	0.99 ± 0.01	55 ± 1
	50	0.95 ± 0.01	66 ± 1
	90	0.78 ± 0.02	49 ± 1
$(Tb_xGd_{1-x})_2(1,4\text{-bdc})_3{\cdot}4H_2O$	1	1.05 ± 0.01	23 ± 1
	10	1.00 ± 0.01	47 ± 1
	50	0.93 ± 0.01	63 ± 1
	90	0.75 ± 0.01	52 ± 1

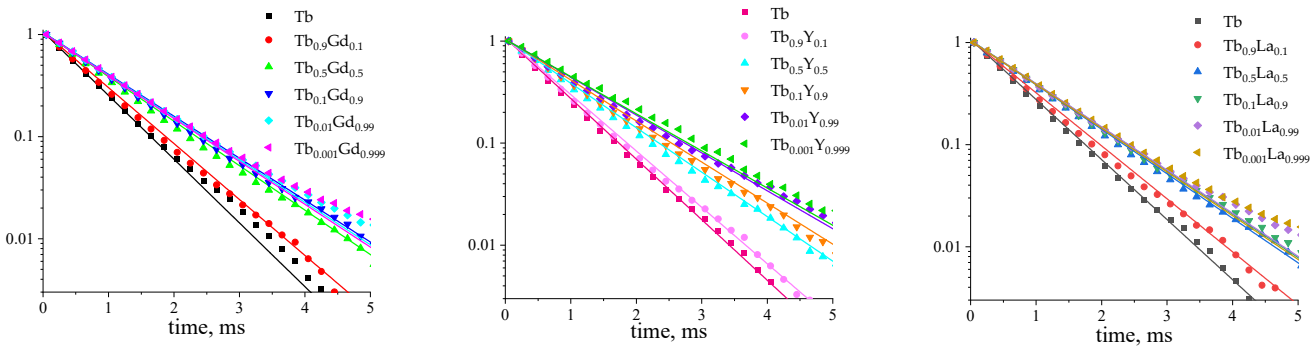

(**a**) (**b**) (**c**)

Figure 6. The photoluminescence decay curves of (**a**) $(Tb_xGd_{1-x})_2(1.4\text{-bdc})_3{\cdot}4H_2O$, (**b**) $(Tb_xY_{1-x})_2(1.4\text{-bdc})_3{\cdot}4H_2O$, and (**c**) $(Tb_xLa_{1-x})_2(1.4\text{-bdc})_3{\cdot}4H_2O$ at the selected concentrations of Tb^{3+} (x = 0.001, 0.01, 0.1, 0.5, 0.9, 1; given in legend) upon 320 nm excitation. *Y*-axis is logarithmic normalized intensity of luminescence.

4. Conclusions

In the current study, the structure and luminescent properties of heterometallic terbium-based terephthalate "antenna" MOFs, namely $(Tb_xM_{1-x})_2(1,4\text{-bdc})_3{\cdot}4H_2O$ (M = Gd, La, Y; x = 0.001–1), were studied in detail in a wide concentration range. The particle morphology, thermal stability, and vibrational structure of the selected homo- and bi-metallic materials are reported as well. All of the compounds studied are isomorphic to each other and correspond to the crystal structure of $Ln_2(1,4\text{-bdc})_3{\cdot}4H_2O$ (Ln = Ce–Yb) [35]. The unit cell parameters of the synthesized compounds were refined using the Pawley method. The unit cell volumes linearly depend on the Tb^{3+} concentration. The substitution of Tb^{3+} ions with La^{3+} ions, which have a larger radius, leads to an increase in the unit cell parameters in the compounds $(Tb_xLa_{1-x})_2(1,4\text{-bdc})_3\ 4H_2O$, whereas replacement of Tb^{3+} with Y^{3+} ions with smaller radii leads to a decrease in the unit cell volumes in the series $(Tb_xM_{1-x})_2(1,4\text{-bdc})_3\ 4H_2O$; for compounds of the series $(Tb_xGd_{1-x})_2(1,4\text{-bdc})_3\ 4H_2O$, the unit cell parameters remain virtually unchanged in the series due to the close values and radii of Tb^{3+} and Gd^{3+}. Thus, Vegard's law is obeyed [37], indicating that the synthesized compounds are solid solutions in a whole concentration range. Using Scanning Electron Microscopy, we revealed that synthesized compounds consist of large particles with an average size of between 5 and 20 μm. The obtained materials have a porous structure (10–200 nm pore size) and consist of aggregated nanoparticles. The IR spectra contains the characteristic bands of the lanthanide-coordinated water molecules and the carboxyl group in the terephthalate ions. The almost identical shape of the IR spectra indicates the similar structure of the synthesized terephthalates. All of the compounds are thermally stable up to 120 °C. Further heating results in dehydration of the compounds, resulting in the formation of anhydrous terephthalates. All of the reported MOFs demonstrate the antenna effect. Their emission spectra consist of narrow bands corresponding to $^5D_4$–^7F_J (J = 3–6) transitions in the Tb^{3+} ion upon 320 nm excitation into a singlet-excited state of the terephthalate ion. The fine structure of the emission spectra for the Tb–Gd, Tb–Y, and Tb–La compound series is identical to that of the unsubstituted $Tb_2(1,4\text{-bdc})_3{\cdot}4H_2O$ emission spectra due to the same local symmetry of Tb^{3+}. This is also confirmed by the identity of the crystalline phase in all of the compounds. Photoluminescence decay and PLQY mostly depend on the dopant concentration, but not on the type of doping ion. The $^5D_4$ excited-state lifetime decreases from 1.1 to 0.7 ms as the Tb^{3+} concentration increases due to concentration quenching. Maximum PLQYs are observed for 50%-substituted solid solutions $(TbM(1,4\text{-bdc})_3{\cdot}4H_2O$ (M = Gd, La, Y); PLQY = 63, 66, and 60% for Gd, La, Y), exceeding the PLQY of unsubstituted terbium terephthalate $(Tb_2(1,4\text{-bdc})_3{\cdot}4H_2O$; PLQY = 46%). Therefore, we have demonstrated, contrary to previous work [24], that the

50% substitution of Tb^{3+} for Y^{3+}, Gd^{3+}, and La^{3+} ions results in a significant enhancement of the photoluminescence quantum yield, up to 1.6 times.

Supplementary Materials: The following supporting information can be downloaded at: https://www.mdpi.com/article/10.3390/cryst14110966/s1, Figure S1: The powder X-ray diffraction (PXRD) patterns of the synthesized compounds series: (a) $(Tb_xGd_{1-x})_2(1,4\text{-bdc})_3\cdot nH_2O$ (x = 0.001–1) including the $Gd_2(1,4\text{-bdc})_3\cdot nH_2O$, (b) $(Tb_xLa_{1-x})_2(1,4\text{-bdc})_3\cdot nH_2O$ (x = 0.001–1) including the $La_2(1,4\text{-bdc})_3\cdot nH_2O$, (c) $(Tb_xY_{1-x})_2(1,4\text{-bdc})_3\cdot nH_2O$ (x = 0.001–1) including the $Y_2(1,4\text{-bdc})_3\cdot nH_2O$. The positions and relative intensities of diffraction maxima of $Tb_2(1,4\text{-bdc})_3\cdot 4H_2O$ taken from ref. [34] are shown as bars, Figure S2: The normalized emission spectra of (a) $(Tb_xGd_{1-x})_2(1,4\text{-bdc})_3\cdot 4H_2O$, (b) $(Tb_xY_{1-x})_2(1,4\text{-bdc})_3\cdot 4H_2O$, (c) $(Tb_xLa_{1-x})_2(1,4\text{-bdc})_3\cdot 4H_2O$ at a wide concentration range of Tb^{3+} (x = 0.001–1; given in legend) upon 320 nm excitation. The artefact maxima peaked at 615 nm (marked as *) correspond to the Eu^{3+} present as impurities in the gadolinium nitrate used for the synthesis, Figure S3: The superimposed emission spectra of (a) $(Tb_xGd_{1-x})_2(1,4\text{-bdc})_3\cdot 4H_2O$, (b) $(Tb_xLa_{1-x})_2(1,4\text{-bdc})_3\cdot 4H_2O$, and (c) $(Tb_xY_{1-x})_2(1.4\text{-bdc})_3\cdot 4H_2O$ at a wide concentration range of Tb^{3+} (x = 0.001–1; given in legend) upon 320 nm excitation, Table S1: Unit cell parameters of the $(Tb_xM_{1-x})_2(1,4\text{-bdc})_3\cdot 4H_2O$ (M = Y, La, Gd; x = 0.04–1). Table S2: Tb^{3+} atomic fractions (at.%) in the synthesized compounds, namely, $(Tb_xM_{1-x})_2(1,4\text{-bdc})_3\cdot 4H_2O$. Measured data were obtained from EDX.

Author Contributions: Conceptualization, A.S.M., A.S.P., and O.S.B.; methodology, A.S.M., Y.N.T., A.S.P., and O.S.B.; validation, M.N.R. and I.E.K.; formal analysis, A.S.M., A.S.P., and O.S.B.; investigation, A.S.M., A.S.P., S.N.O., and O.S.B.; resources, A.S.M., M.Y.S., and N.A.B.; data curation, A.S.M., A.S.P., and O.S.B.; writing—original draft preparation, A.S.M., N.A.B., A.S.P., and O.S.B.; writing—review and editing, M.Y.S., Y.N.T., I.E.K., N.A.B., A.S.P., O.S.B., and A.S.M.; visualization, A.S.M., A.S.P., and O.S.B.; supervision, A.S.M.; project administration, A.S.M.; funding acquisition, A.S.M. All authors have read and agreed to the published version of the manuscript.

Funding: This work was supported by the Russian Science Foundation under grant No. 22-73-10040 (https://rscf.ru/en/project/22-73-10040/, accessed on 16 October 2024).

Data Availability Statement: The original contributions presented in the study are included in the article (and Supplementary Materials), further inquiries can be directed to the corresponding authors.

Acknowledgments: The measurements were performed in the Research Park of Saint Petersburg State University (Magnetic Resonance Research Centre, Chemical Analysis and Materials Research Centre, Cryogenic Department, Interdisciplinary Resource Centre for Nanotechnology, Centre for X-ray Diffraction Studies, Centre for Optical and Laser Materials Research, Thermogravimetric and Calorimetric Research Centre, and Centre for Innovative Technologies of Composite Nanomaterials). This article was published in commemoration of the 300th anniversary of Saint Petersburg State University's founding.

Conflicts of Interest: The authors declare no conflicts of interest.

References

1. Cui, Y.; Chen, B.; Qian, G. Lanthanide Metal–Organic Frameworks for Luminescent Sensing and Light-Emitting Applications. *Coord. Chem. Rev.* **2014**, *273–274*, 76–86. [CrossRef]
2. Chen, B.; Wang, L.; Xiao, Y.; Fronczek, F.R.; Xue, M.; Cui, Y.; Qian, G. A Luminescent Metal–Organic Framework with Lewis Basic Pyridyl Sites for the Sensing of Metal Ions. *Angew. Chem. Int. Ed.* **2009**, *48*, 500–503. [CrossRef] [PubMed]
3. Pellé, F.; Aschehoug, P.; Surblé, S.; Millange, F.; Serre, C.; Férey, G. Interactions between Eu^{3+} Ions in Inorganic-Organic Hybrid Materials. *J. Solid State Chem.* **2010**, *183*, 795–802. [CrossRef]
4. Lee, J.; Farha, O.K.; Roberts, J.; Scheidt, K.A.; Nguyen, S.T.; Hupp, J.T. Metal–Organic Framework Materials as Catalysts. *Chem. Soc. Rev.* **2009**, *38*, 1450–1459. [CrossRef]
5. Massi, M.; Ogden, M.I. Luminescent Lanthanoid Calixarene Complexes and Materials. *Materials* **2017**, *10*, 1369. [CrossRef]
6. Liu, D.; Lu, K.; Poon, C.; Lin, W. Metal–Organic Frameworks as Sensory Materials and Imaging Agents. *Inorg. Chem.* **2014**, *53*, 1916–1924. [CrossRef]
7. Zhou, X.; Wang, H.; Jiang, S.; Xiang, G.; Tang, X.; Luo, X.; Li, L.; Zhou, X. Multifunctional Luminescent Material Eu(III) and Tb(III) Complexes with Pyridine-3,5-Dicarboxylic Acid Linker: Crystal Structures, Tunable Emission, Energy Transfer, and Temperature Sensing. *Inorg. Chem.* **2019**, *58*, 3780–3788. [CrossRef]

8. Shurygin, A.V.; Vovna, V.I.; Korochentsev, V.V.; Mirochnik, A.G.; Kalinovskaya, I.V.; Sergienko, V.I. Optical Properties and Electronic Structure of Eu(III) Complexes with HMPA and TPPO. *Spectrochim. Acta Part A Mol. Biomol. Spectrosc.* **2021**, *250*, 119397. [CrossRef]
9. Khudoleeva, V.; Tcelykh, L.; Kovalenko, A.; Kalyakina, A.; Goloveshkin, A.; Lepnev, L.; Utochnikova, V. Terbium-Europium Fluorides Surface Modified with Benzoate and Terephthalate Anions for Temperature Sensing: Does Sensitivity Depend on the Ligand? *J. Lumin.* **2018**, *201*, 500–508. [CrossRef]
10. Aslandukov, A.N.; Utochnikova, V.V.; Goriachiy, D.O.; Vashchenko, A.A.; Tsymbarenko, D.M.; Hoffmann, M.; Pietraszkiewicz, M.; Kuzmina, N.P. The Development of a New Approach toward Lanthanide-Based OLED Fabrication: New Host Materials for Tb-Based Emitters. *Dalt. Trans.* **2018**, *47*, 16350–16357. [CrossRef]
11. Kozlov, M.I.; Aslandukov, A.N.; Vashchenko, A.A.; Medvedko, A.V.; Aleksandrov, A.E.; Grzibovskis, R.; Goloveshkin, A.S.; Lepnev, L.S.; Tameev, A.R.; Vembris, A.; et al. On the Development of a New Approach to the Design of Lanthanide-Based Materials for Solution-Processed OLEDs. *Dalt. Trans.* **2019**, *48*, 17298–17309. [CrossRef] [PubMed]
12. Girotto, E.; Pereira, A.; Arantes, C.; Cremona, M.; Bortoluzzi, A.J.; Salla, C.A.M.; Bechtold, I.H.; Gallardo, H. Efficient Terbium Complex Based on a Novel Pyrazolone Derivative Ligand Used in Solution-Processed OLEDs. *J. Lumin.* **2019**, *208*, 57–62. [CrossRef]
13. Sravani, V.V.; Gupta, S.K.; Sreenivasulu, B.; Gangopadhyay, P.; Rao, C.V.S.B.; Suresh, A.; Sivaraman, N. Bright Green Emitting Terbium-MOF with High Quantum Yield Achieved through Post Synthetic Modifications. *Opt. Mater.* **2022**, *133*, 112944. [CrossRef]
14. Özgür, E.; Patra, H.K.; Turner, A.P.F.; Denizli, A.; Uzun, L. Lanthanide [Terbium(III)]-Doped Molecularly Imprinted Nanoarchitectures for the Fluorimetric Detection of Melatonin. *Ind. Eng. Chem. Res.* **2020**, *59*, 16068–16076. [CrossRef]
15. Zhang, Z.; Zhang, L.; Han, P.; Liu, Q. A Luminescent Probe Based on Terbium-Based Metal–Organic Frameworks for Organophosphorus Pesticides Detection. *Microchim. Acta* **2022**, *189*, 438. [CrossRef]
16. Yang, M.; Shi, J.; Luo, T.; Yang, X. Luminescence Detection of Cr^{3+}, Bi^{3+}, and Acetone in Aqueous Solution by Core-Shell Tb-MOF. *Curr. Anal. Chem.* **2025**, *21*, 57–67. [CrossRef]
17. Wang, X.; Cong, Q.; Feng, C.; Sun, Z.; Cai, Z.; Fan, C.; Pei, L. Terbium Vanadate Nanowires-Based Electrochemical Sensors for Mercury Ions. *Appl. Biochem. Biotechnol.* **2024**. [CrossRef]
18. Yue, X.; Fu, L.; Li, Y.; Xu, S.; Lin, X.; Bai, Y. Lanthanide Bimetallic MOF-Based Fluorescent Sensor for Sensitive and Visual Detection of Sulfamerazine and Malachite. *Food Chem.* **2023**, *410*, 135390. [CrossRef]
19. Yin, H.Q.; Wang, X.Y.; Yin, X.B. Rotation Restricted Emission and Antenna Effect in Single Metal–Organic Frameworks. *J. Am. Chem. Soc.* **2019**, *141*, 15166–15173. [CrossRef]
20. Cao, W.; Tang, Y.; Cui, Y.; Qian, G. Energy Transfer in Metal–Organic Frameworks and Its Applications. *Small Struct.* **2020**, *1*, 2000019. [CrossRef]
21. Alpha, B.; Ballardini, R.; Balzani, V.; Lehn, J.-M.; Perathoner, S.; Sabbatini, N. Antenna Effect in Luminescent Lanthanide Cryptates: A Photophysical Study. *Photochem. Photobiol.* **1990**, *52*, 299–306. [CrossRef]
22. Kolesnik, S.S.; Nosov, V.G.; Kolesnikov, I.E.; Khairullina, E.M.; Tumkin, I.I.; Vidyakina, A.A.; Sysoeva, A.A.; Ryazantsev, M.N.; Panov, M.S.; Khripun, V.D.; et al. Ultrasound-Assisted Synthesis of Luminescent Micro-and Nanocrystalline Eu-Based Mofs as Luminescent Probes for Heavy Metal Ions. *Nanomaterials* **2021**, *11*, 2448. [CrossRef] [PubMed]
23. Orlova, A.V.; Kozhevnikova, V.Y.; Lepnev, L.S.; Goloveshkin, A.S.; Le-Deigen, I.M.; Utochnikova, V.V. NIR Emitting Terephthalates $(Sm_xDy_yGd_{1-x-y})_2(Tph)_3(H_2O)_4$ for Luminescence Thermometry in the Physiological Range. *J. Rare Earths* **2020**, *38*, 492–497. [CrossRef]
24. Utochnikova, V.V.; Kuzmina, N.P. Photoluminescence of Lanthanide Aromatic Carboxylates. *Russ. J. Coord. Chem. Khimiya* **2016**, *42*, 679–694. [CrossRef]
25. Wang, P.; Li, Z.F.; Song, L.P.; Wang, C.X.; Chen, Y. Catena-Poly[[[μ-Benzene-1,4-Dicarboxylato-Bis[Tetraaqualutetium(III)]] -Di-μ-Benzene-1,4-Dicarboxylato] Dihydrate]. *Acta Crystallogr. Sect. E Struct. Rep. Online* **2006**, *62*, 253–255. [CrossRef]
26. Do Nascimento, J.F.S.; De Araújo, A.M.U.; Kulesza, J.; De Farias Monteiro, A.F.; Júnior, S.A.; Barros, B.S. Solid-State Tunable Photoluminescence in Gadolinium-Organic Frameworks: Effects of the Eu^{3+} Content and Co-Doping with Tb^{3+}. *New J. Chem.* **2018**, *42*, 5514–5522. [CrossRef]
27. Nosov, V.G.; Kupryakov, A.S.; Kolesnikov, I.E.; Vidyakina, A.A.; Tumkin, I.I.; Kolesnik, S.S.; Ryazantsev, M.N.; Bogachev, N.A.; Skripkin, M.Y.; Mereshchenko, A.S. Heterometallic Europium(III)–Lutetium(III) Terephthalates as Bright Luminescent Antenna MOFs. *Molecules* **2022**, *27*, 5763. [CrossRef]
28. Nosov, V.G.; Toikka, Y.N.; Petrova, A.S.; Butorlin, O.S.; Kolesnikov, I.E.; Orlov, S.N.; Ryazantsev, M.N.; Kolesnik, S.S.; Bogachev, N.A.; Skripkin, M.Y.; et al. Brightly Luminescent $(Tb_xLu_{1-x})_2bdc_3{\cdot}nH_2O$ MOFs: Effect of Synthesis Conditions on Structure and Luminescent Properties. *Molecules* **2023**, *28*, 2378. [CrossRef]
29. Kolesnik, S.S.; Bogachev, N.A.; Kolesnikov, I.E.; Orlov, S.N.; Ryazantsev, M.N.; González, G.; Skripkin, M.Y.; Mereshchenko, A.S. Microcrystalline Luminescent $(Eu_{1-x}Ln_x)_2bdc_3{\cdot}nH_2O$ (Ln = La, Gd, Lu) Antenna MOFs: Effect of Dopant Content on Structure, Particle Morphology, and Luminescent Properties. *Molecules* **2024**, *29*, 532. [CrossRef]
30. Toikka, Y.N.; Badikov, A.R.; Bogachev, N.A.; Kolesnikov, I.E.; Skripkin, M.Y.; Orlov, S.N.; Mereshchenko, A.S. Luminescent Properties and Thermal Stability of $(Lu_{0.98}Eu_{0.02})_2bdc_3{\cdot}10H_2O$ Metal–Organic Frameworks. *Mendeleev Commun.* **2024**, *34*, 634–636. [CrossRef]

31. Butorlin, O.S.; Petrova, A.S.; Toikka, Y.N.; Kolesnikov, I.E.; Orlov, S.N.; Ryazantsev, M.N.; Bogachev, N.A.; Skripkin, M.Y.; Mereshchenko, A.S. The Structure and Optical Properties of Luminescent Europium Terephthalate Antenna Metal–Organic Frameworks Doped by Yttrium, Gadolinium, and Lanthanum Ions. *Molecules* **2024**, *29*, 3558. [CrossRef] [PubMed]
32. Utochnikova, V.V.; Grishko, A.Y.; Koshelev, D.S.; Averin, A.A.; Lepnev, L.S.; Kuzmina, N.P. Lanthanide Heterometallic Terephthalates: Concentration Quenching and the Principles of the "Multiphotonic Emission". *Opt. Mater.* **2017**, *74*, 201–208. [CrossRef]
33. Alammar, T.; Hlova, I.Z.; Gupta, S.; Biswas, A.; Ma, T.; Zhou, L.; Balema, V.; Pecharsky, V.K.; Mudring, A.V. Mechanochemical Synthesis, Luminescent and Magnetic Properties of Lanthanide Benzene-1,4-Dicarboxylate Coordination Polymers $(Ln_{0.5}Gd_{0.5})_2$ $(1,4\text{-BDC})_3(H_2O)_4$; Ln = Sm, Eu, Tb. *New J. Chem.* **2020**, *44*, 1054–1062. [CrossRef]
34. Haquin, V.; Etienne, M.; Daiguebonne, C.; Freslon, S.; Calvez, G.; Bernot, K.; Le Pollès, L.; Ashbrook, S.E.; Mitchell, M.R.; Bünzli, J.C.; et al. Color and Brightness Tuning in Heteronuclear Lanthanide Terephthalate Coordination Polymers. *Eur. J. Inorg. Chem.* **2013**, *2013*, 3464–3476. [CrossRef]
35. Reineke, T.M.; Eddaoudi, M.; Fehr, M.; Kelley, D.; Yaghi, O.M. From Condensed Lanthanide Coordination Solids to Microporous Frameworks Having Accessible Metal Sites. *J. Am. Chem. Soc.* **1999**, *121*, 1651–1657. [CrossRef]
36. Pawley, G.S. Unit-cell refinement from powder diffraction scans. *J. Appl. Crystallogr.* **1981**, *14*, 357–361. [CrossRef]
37. Denton, A.R.; Ashcroft, N.W. Vegard's Law. *Phys. Rev. A* **1991**, *43*, 3161–3164. [CrossRef]
38. Shannon, R.D. Revised Effective Ionic Radii and Systematic Studies of Interatomic Distances in Halides and Chalcogenides. *Acta Crystallogr.* **1976**, *A32*, 751–767. [CrossRef]
39. Costa, B.A.; Nunes, W.D.G.; Bembo, L.H.; Siqueira, A.B.; Caires, F.; Leles, M.I.G.; Ionashiro, E.Y. Study of Thermoanalytical Behavior of Heavier Lanthanides Terephthalates in Air Atmosphere. *J. Therm. Anal. Calorim.* **2018**, *134*, 1205–1210. [CrossRef]
40. Nunes, W.D.G.; Teixeira, J.A.; do Nascimento, A.L.C.S.; Caires, F.J.; Ionashiro, E.Y.; Ionashiro, M. A Comparative Study on Thermal Behavior of Solid-State Light Trivalent Lanthanide Isonicotinates in Dynamic Dry Air and Nitrogen Atmospheres. *J. Therm. Anal. Calorim.* **2016**, *125*, 397–405. [CrossRef]
41. Daiguebonne, C.; Kerbellec, N.; Guillou, O.; Bünzli, J.C.; Gumy, F.; Catala, L.; Mallah, T.; Audebrand, N.; Gérault, Y.; Bernot, K.; et al. Structural and Luminescent Properties of Micro- and Nanosized Particles of Lanthanide Terephthalate Coordination Polymers. *Inorg. Chem.* **2008**, *47*, 3700–3708. [CrossRef]
42. Latva, M.; Takalob, H.; Mukkala, V.M.; Matachescu, C.; Rodríguez-Ubis, J.C.; Kankare, J. Correlation between the Lowest Triplet State Energy Level of the Ligand and Lanthanide(III) Luminescence Quantum Yield. *J. Lumin.* **1997**, *75*, 149–169. [CrossRef]
43. Binnemans, K. Interpretation of Europium(III) Spectra. *Coord. Chem. Rev.* **2015**, *295*, 1–45. [CrossRef]
44. Holsa, J.; Leskela, M.; Niinisto, L. Concentration quenching of Tb^{3+} luminescence in laobr and Gd202S phosphors. *Mat. Res. Bull.* **1979**, *14*, 1403–1409. [CrossRef]
45. Zhang, W.; Kou, H.; Ge, L.; Zhang, Y.; Lin, L.; Li, W. Effects of Doping Ions on the Luminescence Performance of Terbium Doped Gadolinium Polysulfide Phosphor. *J. Phys. Conf. Ser.* **2020**, *1549*, 032064. [CrossRef]
46. Kolesnikov, I.E.; Mamonova, D.V.; Lähderanta, E.; Kurochkin, A.V.; Mikhailov, M.D. The Impact of Doping Concentration on Structure and Photoluminescence of Lu_2O_3:Eu^{3+} Nanocrystals. *J. Lumin.* **2017**, *187*, 26–32. [CrossRef]
47. Kolesnikov, I.E.; Kalinichev, A.A.; Kurochkin, M.A.; Golyeva, E.V.; Terentyeva, A.S.; Kolesnikov, E.Y.; Lähderanta, E. Structural, Luminescence and Thermometric Properties of Nanocrystalline YVO_4:Dy^{3+} Temperature and Concentration Series. *Sci. Rep.* **2019**, *9*, 2043. [CrossRef]